https://doi.org/10.5194/egusphere-2024-1885
Preprint. Discussion started: 1 July 2024

Grounded ridge detection and characterization along the Alaskan Arctic coastline using ICESat-2 surface height retrievals

Kennedy A. Lange[1], Alice C. Bradley[1], Kyle Duncan[2], and Sinéad L. Farrell[3]

[1]Geoscience Department, Williams College, 18 Hoxsey St. Williamstown, MA, USA
[2]Earth System Science Interdisciplinary Center (ESSIC), University of Maryland College Park, College Park, USA
[3]Department of Geographical Sciences, University of Maryland College Park, College Park, USA

Correspondence: Alice Bradley (alice.c.bradley@williams.edu)

Abstract. Grounded sea ice ridges are an important morphological feature that stabilize shorefast ice along Arctic coastlines. Investigating the development of shorefast ice around Utqiaġvik, AK, we employ high-resolution altimetry data from NASA's ICESat-2 satellite to describe an approach to identify grounded ridges and to track the development of shorefast ice over the winter season. We apply the University of Maryland Ridge Detection Algorithm (Duncan and Farrell, 2022) using ICESat-2 ATL03 elevation data to identify and calculate ridge sail heights and estimate ridge depths using empirical relationships based on first-year ice ridge geometries surveyed in the Beaufort, Chukchi, and Bering Seas. The estimated ridge depths are then compared with 15 arc-second resolution bathymetric data from the General Bathymetric Chart of the Oceans (GEBCO) to detect likely grounded ridges. This approach for identifying and characterizing grounded ridges in shorefast ice is then applied across the entire Alaskan Arctic coastline in the 2021-2022 winter to characterize grounded ridge depth, height, width, number of ridges per track, and distance from shore. We find that distributions in ridge grounding depth skew towards shallower water and ridges are narrower and closer to shore on the Chukchi side of the Alaskan Arctic. Mean grounding depths of 5.4 m in the Chukchi and 9.1 m in the Beaufort are notably shallower than the traditional "stamuki" zone ($\geq$10 m). With further application of the methods demonstrated here, we can begin to map patterns in shorefast ice stability, seasonality, and improve our understanding of near-shore ice dynamics across Arctic coastal regions in a changing climate.

1 Introduction

Coastal sea ice serves as an important barrier between the shoreline and drifting pack ice. Stable landfast ice not only shields the coastline from erosion caused by winter storms (Hošeková et al., 2021; Lantuit and Pollard, 2008; Overeem et al., 2011; Zhang et al., 2004), but also provides a stable surface for transportation between towns, to and from the flaw leads throughout the winter (Baztan et al., 2017), and out to off-shore drill rigs (Potter et al., 1981; Masterson, 2009). Indigenous communities and mammals rely on this stable ice for food security and sustenance from hunting migratory marine species (Huntington et al., 2022; Laidre et al., 2008; Laidler et al., 2009), birds (Lovvorn et al., 2018), and bowhead whale (Druckenmiller et al., 2010).

An increase in ice breakout events and shorter shorefast ice seasons during recent years endangers hunters whose safety depends on knowledge of ice dynamics (Gearheard et al., 2006; Mahoney et al., 2014; George et al., 2004). Since 1980, the volume of ice in the Arctic Ocean is thought to have declined by 75% (Overland et al., 2014), and observations show that later

https://doi.org/10.5194/egusphere-2024-1885
Preprint. Discussion started: 1 July 2024

ice freeze-ups and earlier thaws are occurring throughout the Arctic as a result of shortening winters (Mahoney et al., 2014; Stammerjohn et al., 2012), thinning ice (Kwok et al., 2009; Rothrock et al., 1999; Laxon et al., 2013; Mahoney et al., 2009; Howell et al., 2016; Gerland et al., 2008), and increasingly unstable ice conditions (Meier et al., 2006).

Grounded ridges play a crucial role in stabilizing shorefast ice, so better information about the state of grounded ridges at both local and pan-Arctic scales can inform decision making around the use of the coastal zone (Eicken et al., 2009). These ridges form when drifting pack ice collides with bottomfast ice attached to shore, as shown in Figure 1(A). If this collision occurs at the correct angles and the ice attached to the shore does not break off, deformation ridges form at this boundary (B). Some of these ridges are deep enough that they anchor the landfast ice in the sea floor (C), forming a grounded ridge. The stabilizing mechanism in landfast ice, illustrated in the cross-sectional view on Figure 1, relies on attachment points of the ice both from bottomfast ice along the shoreline and the grounded ridge keel (H_k). Grounded ridges form either when a compression ridge drifts into shallower waters and gets stuck in the sea floor or from an in situ collision between the shorefast ice and drifting pack ice (Mahoney et al., 2007b; Jones et al., 2016; Reimnitz et al., 1978). These stable ridges protect the shorefast ice from drifting pack ice, keeping it immobile until breakup occurs in the spring (Jones et al., 2016). The rates and mechanisms of shorefast ice breakup are determined by the presence and location of grounded ridges (Petrich et al., 2012).

Where a ridge grounds relative to shore depends on several factors: the local bathymetry (water must be shallow enough for the ice to reach the sea floor (Selyuzhenok et al., 2015)), the thickness of the ice (seasonal timing of ridge formation), the direction and momentum of drifting pack ice causing the collision event, and the chance location of weak points in the shore ice allowing for brittle failure and ridge formation (Jones et al., 2016). There are both geographic patterns (e.g., bathymetry, aspect of shoreline relative to dominate ice drift direction) and stochastic processes (e.g., weather, timing of freeze-up, and rate of ice growth) influencing the location of grounded ridges in any given winter season. Assuming some typical sea ice thickness and pack ice momentum, there is a bathymetric depth, called the “stamuki” zone, where the probability of a ridge becoming grounded becomes reasonably high. Over the years, it has been defined in multiple ways: between 15-50 m depths (Barnes et al., 1987), around the 20 m isobath (Barnes et al., 1982), 10-27 m water based on field observations in 1983 (McGonigal and Barrette, 2018). In our analysis, we define the “stamuki" zone as grounding depths greater than 10 m (Reimnitz et al., 1978).

The location of the landfast ice edge can be identified in satellite products including synthetic aperture radar (SAR, e.g., Meyer et al. (2011); Mahoney et al. (2014)), optical imagery including MODIS (Moderate Resolution Imaging Spectroradiometer e.g., Cooley and Ryan (2024)), and Landsat (e.g. Barry et al. (1979)), and field methods such as electromagnetic ice thickness surveys (e.g. Selyuzhenok et al. (2017)). Studies and observations have documented the extent of land-fast ice (Dammann et al., 2019; Selyuzhenok et al., 2015), including significant reductions in land-fast ice thickness (George et al., 2004; Mahoney et al., 2009; Gerland et al., 2008) and a shortening stable ice season (Cooley et al., 2020; Meyer et al., 2011; Jensen et al., 2020; Mahoney et al., 2007a). Cooley et al. (2020) suggests that under a modeled high emission scenario (RCP8.5), the spring shore-fast ice season will see between a 5 and 44 day reduction in length by 2100. Other studies have found similar results where shore-fast ice seasons are more variable and shortening in duration by around -7 ($\pm$1.5)% per decade (Yu et al., 2014) or by 2.8 days per year (Selyuzhenok et al., 2015).

https://doi.org/10.5194/egusphere-2024-1885
Preprint. Discussion started: 1 July 2024

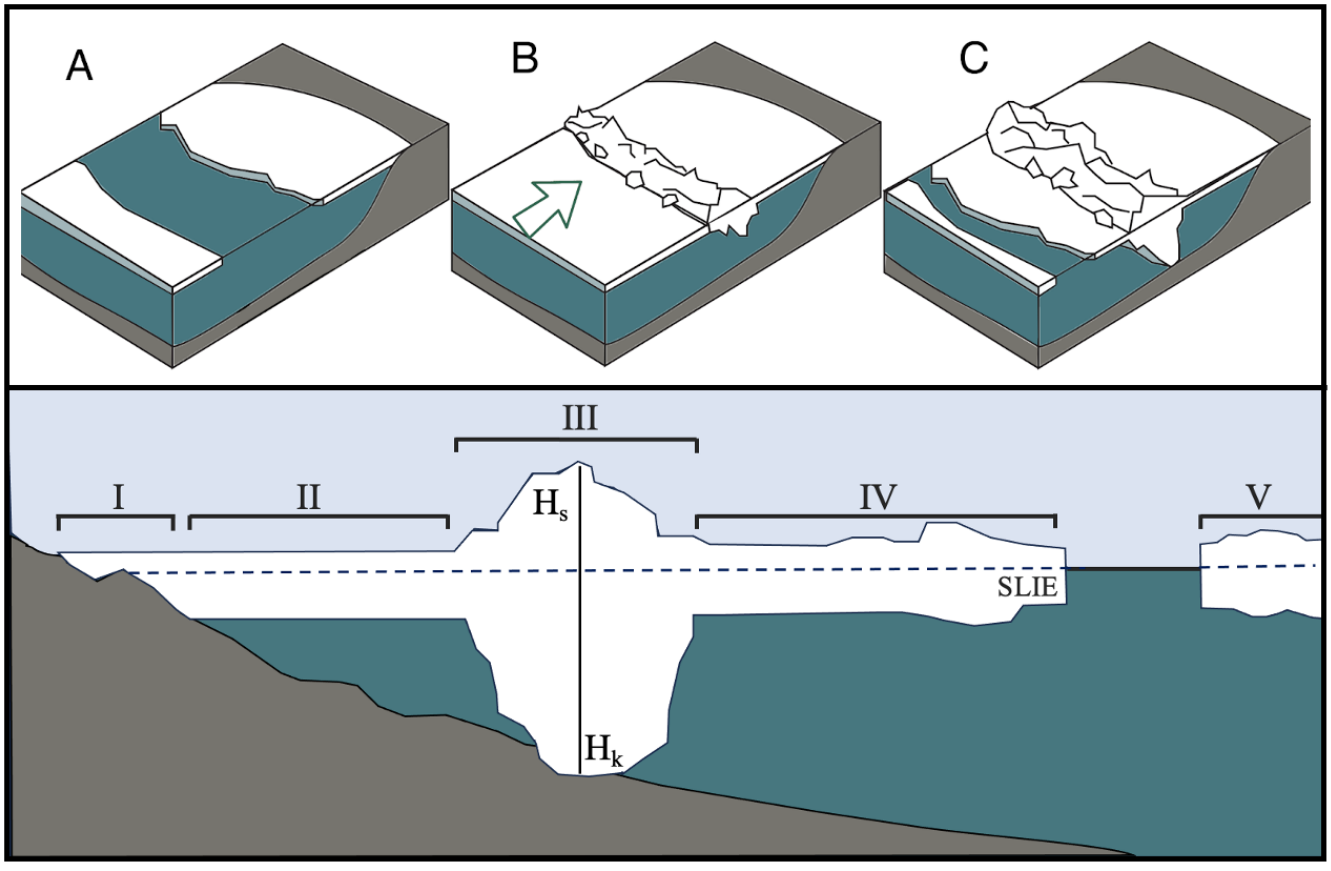

Figure 1. The grounded ridge formation process, with (A) the formation of bottom-fast ice attached to shore, (B) drifting pack ice colliding to form a deformation ridge, and (C) that ridge building deep enough to embed in the sea floor. The lower panel shows a cross section of a grounded ice ridge during the winter, not to scale. I is bottomfast ice, II is grounded shorefast ice, III is the grounded ridge, IV is the landfast ice extension, and V is drifting pack ice. The seaward landfast ice edge (SLIE) represents the boundary between shorefast ice and a flaw lead or drifting pack ice. Ridge sail height (H_s) and keel depth (H_k) are labeled relative to water level.

https://doi.org/10.5194/egusphere-2024-1885
Preprint. Discussion started: 1 July 2024

Determining whether a particular ridge is grounded has previously required in situ manual measurement or under-ice sensors, and many such surveys predate modern open data policies. Data from the Utqiaġvik sea ice radar system has enabled observations of ridge formation (Mahoney et al., 2007b), though this approach still does not necessarily confirm whether ridges are grounded, and relies upon substantial infrastructure in the form of the sea ice radar system that cannot be applied broadly in more remote regions. Past studies have used remote sensing data to document the stability of ice by measuring movement over time, since ice that remains motionless for extended periods is likely to be grounded in the sea floor (Jones et al., 2016; Meyer et al., 2011). Remote sensing of the Arctic region is limited by persistent cloud cover, polar night, low-resolution products incapable of resolving small scale ice features, and few satellites that operate on polar orbits. These limitations underscore the importance of developing a method to identify and monitor grounded ridges, as their importance to Arctic communities surpasses the limited attention they have received in the literature.

In this paper, we present a novel method for identifying grounded ridges in shorefast ice over the course of a winter season. We detect individual ridges in ICESat-2 laser altimetry profiles of surface height using the University of Maryland Ridge Detection Algorithm (UMD-RDA) (Duncan and Farrell, 2022), and estimate their keel depths using empirical relationships of ridge geometries from observed first-year ice ridges in the region. We show that this approach can be used to identify grounded ridges that either persist over time, or are newly grounded, and correspond to features identified in Sentinel-1 SAR imagery. This method was developed using two pilot study areas outside Utqiaġvik, Alaska and then applied across the Alaskan Arctic coastline to survey grounded ridges during 2021-2022 winter season. From this analysis, we characterize Arctic grounded ridges and enhance our understanding of Arctic shorefast ice dynamics.

2 Data

We identified two pilot study areas outside Utqiaġvik Alaska that are 10x20 km on the Chukchi Sea side and 20 x 30 km on the Beaufort Sea side of Point Barrow, indicated in Figure 2. These areas provide two different bathymetric profiles in a geographically proximal locations with different characteristic ice drift directions. After demonstrating the approach, we extend the analysis along Alaskan Arctic coastline from Point Hope, AK to Komakuk Beach, Canada to survey ridges on a broader scale. While this represents only a small portion of the Arctic, through the analysis of 1293 ICESat-2 ground tracks along the roughly 1,500 km of coastline, we derive insights into the characteristics of grounded sea ice ridges.

In this study, we analyzed ICESat-2 (Ice, Cloud, and Land Elevation Satellite 2) and Global Elevation Bathymetric Chart of the Oceans (GEBCO) data over the 2021-2022 winter to detect grounded ridges and confirm that the stabilized ice is stationary through the winter. Sentinel-1 data further validates that the associated features are stationary and can better constrain the timing of ridge formation.

2.1 ICESat-2 retrievals

ICESat-2 is a NASA Earth observing satellite, launched in 2018, equipped with an Advanced Topographic Laser Altimeter System (ATLAS), a six-beam laser altimeter arranged in three pairs of strong and weak beams, spaced 3.3 km apart, to

https://doi.org/10.5194/egusphere-2024-1885
Preprint. Discussion started: 1 July 2024

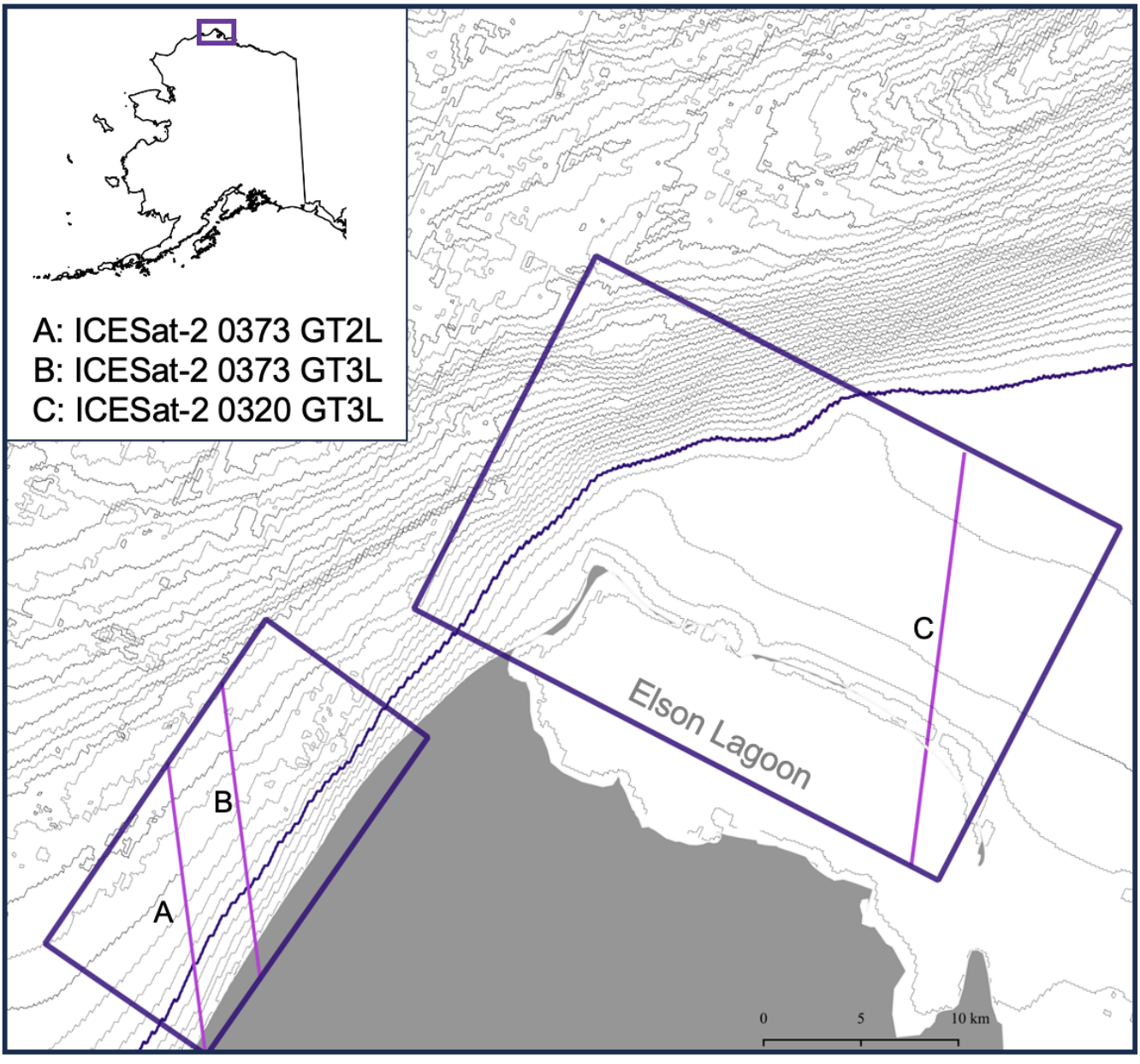

Figure 2. An overview of the pilot study areas offshore of Utqiaġvik, AK (inset map), and the three ICESat-2 ground tracks (GT) labeled A-C (pink lines) highlighted in the results. Bathymetric contours (grey lines) are located every 5m, including the 20m isobath outlined in purple

https://doi.org/10.5194/egusphere-2024-1885
Preprint. Discussion started: 1 July 2024

measure the topographic height of Earth's surface with a footprint resolution of 11 m spaces 0.7 m apart (Magruder et al., 2024). This instrument is the only satellite-based altimetry system that operates at a high-enough spatial resolution to detect individual pressure ridges (Farrell et al., 2020).

We use the University of Maryland Ridge Detection Algorithm (UMD-RDA, Duncan and Farrell (2022)) to extract surface height from ICESat-2's Level 2A Geolocated Photon Data product (ATL03) between December 2021 and May 2022. In filtering background photons, the algorithm detects sea ice height along each track and uses the Rayleigh criterion to detect individual ridge sails (Duncan and Farrell, 2022). The ICESat-2 UMD-RDA results were validated using using independent near-coincident airborne laser scanner data which showed strong correlation (Duncan and Farrell, 2022) but showed that the algorithm underestimates total sail height by ∼0.1 m (Ricker et al., 2023). For the purposes of this analysis, underestimating sail height slightly is preferable to overestimating: with this magnitude of error we are not likely to miss too many grounded ridges.

There were 16 ICESat-2 tracks that intersect the shoreline in the Chukchi study area and 27 in the Beaufort Sea study area (Figure 2) during the 2021-2022 winter season. Because the satellite orbits on a 91-day repeat, there are a maximum of two passes per winter season over the same location. In the area surrounding Utqiaġvik, repeat passes occur in January and April or February and May. However, we found the May passes in the Beaufort pilot area return very little data, likely due to thick cloud cover and/or inclement weather. As a result, there were only seven pairs of repeat satellite passes between the two pilot areas that returned sufficient data to detect individual ridges on both dates, intersected with shore in the study area to provide near-shore measurements, and had two tracks within the period of continuous ice cover to determine whether ridges persist over the 91 day period (Table 1).

Sea	Track	Cycle	Seg	Laser	Dates
Chukchi	0381	14,15	05	GT3L	16 Jan, 17 Apr
Chukchi	0373	14,15	03	GT2L	15 Jan, 16 Apr
Chukchi	0373	14,15	03	GT3L	15 Jan, 16 Apr
Chukchi	0815	14,15	03	GT1L	13 Feb, 15 May
Chukchi	0815	14,15	03	GT2L	13 Feb, 15 May
Beaufort	0320	14,15	05	GT3L	12 Jan, 13 Apr
Beaufort	0381	14,15	05	GT1L	16 Jan, 17 Apr

Table 1. ICESat-2 track specifications for repeated ground tracks (GT) with sufficient available surface height data over study regions during winter 2022.

2.2 Synthetic Aperture Radar

Sentinel-1 is a set of satellites, launched in 2014 and 2016 as part of the ESA Copernicus program, equipped with a C-band Synthetic Aperture Radar Instrument. The low temporal resolution of the ICESat-2 product requires a higher temporal

https://doi.org/10.5194/egusphere-2024-1885
Preprint. Discussion started: 1 July 2024

resolution product to track ice features seasonally: a Sentinel-1 ground track covers the pilot sites once every 12 days. We used Level 1 Ground Range Detected (GRD) radar data with a spatial resolution of 20 x 22 m. Although the spatial resolution is too low to identify most pressure ridges, we can identify persistent features as a proxy for ice stability and therefor infer the presence of grounded ridges. In doing so, we can narrow down the timing of formation and breakup of grounded ridges to a 12 day window, providing information on sea ice stability and persistence on a seasonal scale.

2.3 Bathymetry

In order to determine if a ridge is grounded, it is necessary to have a measure of the sea floor depth. For this analysis, we use the Global Elevation Bathymetric Chart of the Oceans (GEBCO) product (GEBCO Compilation Group, 2023), a dataset that combines available bathymetric surveys regardless of sampling methods. This data is gridded to a 15 arc-second interval grid ($\sim$ 500 m). While higher resolution data products exist (e.g., NCEI Digital Elevation Model Global Mosaic at a grid resolution of 1/3 arcsec $\sim$ 10m), we find the higher resolution both limits the speed and extent of processing while also appearing poorly interpolated in some areas of coastal Alaska. The gridded GEBCO product is sampled along the ICESat-2 tracks with a 2D linear interpolation at the horizontal position of each altimetry measurement.

Beyond the poor spatial resolution of the gridded product, bathymetric data in nearshore areas inherently contains uncertainties due to limited boat access in shallow marine environments. Typical survey approaches do not work, leading to reliance on interpolations from sea floor measurements conducted further offshore in comparison with land based topographic measurements (Amante, 2018). Even with a limited tidal range of 20 cm near Utqiaġvik (NOAA, 2010), tides represent a large fraction of the total depth in shallow water. Moreover, near-shore areas are subject to active sediment transport and redistribution, influenced by wave action, coastal erosion, and scouring from grounded ice. These uncertainties are acknowledged in this study and the results are interpreted accordingly.

3 Analysis

We define sea level relative to the retrieved ice surface height based on the thickness of undeformed ice estimated using a freezing degree day model (Anderson, 1961; Maykut and Untersteiner, 1986; Kaleschke et al., 2012). Using linear regressions on a dataset of surveyed ridge geometry from locations in the Chukchi, Bering, and Beaufort Seas (Appendix, Strub-Klein and Sudom (2012)), we estimate the keel depth from each sail height for each point in the UMD-RDA ICESat-2 retrievals. By comparing the estimated keel depths to the depth of the sea floor interpolated from bathymetric data, we can determine whether the ridges are likely to be grounded.

We consider the two sets of repeat tracks on the Chukchi side of Utqiaġvik and one set on the Beaufort side to demonstrate the capabilities of the algorithm in (1) detecting persistent grounded ridges, (2) detecting changes in grounded ridges, and (3) comparing the Chukchi and Beaufort Sea ice deformation characteristics. We use repeat tracks to confirm that ridges identified as grounded in the early-winter track (January) are still in place in the late-winter track (April), and more generally, to better understand when grounded ridges are forming during the winter season. When we identify immobile land-fast ice in both the

https://doi.org/10.5194/egusphere-2024-1885
Preprint. Discussion started: 1 July 2024

January and April ICESat-2 tracks as indicated by persistent ridges, we can be sure that the ice is stabilized off-shore by a grounded ridge.

Persistent features in the ice can serve as an indicator of ice stability, as grounded ridges act as a stabilizing mechanism throughout the winter season (Jones et al., 2016). In monitoring formation and breakup of features in the SAR imagery, we can narrow down formation and breakup to within approximately two week periods, depending on the availability of repeat images. We use Sentinel-1 SAR imagery to validate the stability of ice features surrounding the grounded ridges detected in the ICESat-2 retrievals.

This approach permits a characterization of grounded ridge geometry and location along Arctic coastlines. We process data from 1271 ICESat-2 tracks (527 in the Chukchi Sea, and 744 in the Beaufort Sea) that intersect the coastline between Point Hope, AK and Komakuk Beach, Canada between December 1st, 2021 and May 1st, 2022. For each identified ridge, we quantify grounded ridge height, bathymetric depth, distance from shore, width, the number of ridges in the shorefast ice, and location relative to shore and the landfast ice edge.

3.1 Freezing degree day model to estimate ice thickness

An accurate estimate of keel depth relies upon a precise alignment of water level relative to the sea ice surface height measurements. The empirical ratios between sail height and keel depth are based on a freeboard measurement. Without reliable lead detection nearby on a particular ICESat-2 track, we estimate undeformed thermodynamically-grown sea ice freeboard using a freezing degree-day (FDD) model for ice thickness and determine water level assuming buoyant equilibrium.

We modeled FDD ice thickness using daily average temperature data for five locations across the Alaskan Arctic: Kotzebue, Utqiaġvik, Komakuk Beach, Kaktovik/Barter Island, and Prudhoe Bay (NOAA, 2024). These sites provide daily temperature data during the period of October 1, 2021 to May 1, 2022 and are spaced along the entire coastline. Equation 1 calculates the number of freezing degree days (Θ) from the freezing point of seawater ($T_f = -1.9$ C) and the daily (or hourly) 2 m air temperature (T_a) integrated over time (t) from an initial freeze up date (D_0) to the date of the measurement (D_1).

$$\Theta = \int_{D_0}^{D_1} (T_f - T_a) dt \tag{1}$$

The ice thickness result depends upon the start date of the model, which is the date in which ice forms that persists through the winter season. Finding this date is complicated because early season ice is prone to breakout events. Starting the model too late would underestimate the ice thickness. Detailed community-based ice observations near Utqiaġvik record the beginning of the landfast ice growth season with “stationary ice along shore" on November 15th, 2021 (Observers Billy Adams and Joe Leavitt, Adams and Observers of coastal Arctic Alaska (2022)), but documented landfast ice formation dates are not available across the entire Arctic Alaskan coastline. Integrating FDD data from a range of possible start dates (D_0 = October 15, November 1, and November 15) provides a likely range of ice thicknesses given the observed weather patterns.

https://doi.org/10.5194/egusphere-2024-1885
Preprint. Discussion started: 1 July 2024

$$H^2 + 5.1H = 6.7\Theta \tag{2}$$

$$H = 1.33\Theta^{0.58} \tag{3}$$

Equation 2 (Anderson, 1961; Maykut and Untersteiner, 1986) and 3 (Kaleschke et al., 2012) calculate ice thickness (H) using two different FDD models. Late in the season there is little difference between the models, but the estimated ice thicknesses vary by up to 10 cm in January. For example, with a start date of November 15, we calculated a thermodynamic ice thickness of 84.37 cm and 90.12 cm on January 15 2022 and 146.43 cm and 146.48 cm on April 16 2022 for Equation 2 and Equation 3 respectively.

3.2 Sail-keel depth relationship estimates

We determine an empirical equation linking ridge sail height to keel depth from field observations. Strub-Klein and Sudom (2012) published a database of ridge measurements including 147 first-year ice ridges surveyed between 1976 and 2008 in areas near the Alaskan Arctic. Ridge locations are indicated by basin, and we consider ridges in the Beaufort and the Chukchi/Bering (grouped in the dataset) regions.

Determining whether a near-shore ridge is grounded depends on the relationship between sail height (H_s) and keel depth (H_k). Because ridge sizes are influenced by a number of factors including floe momentum and the thickness of the parent ice floe, this ratio varies with geographic location (Yu et al., 2014). A Wilcoxon test p-value of 0.01 indicates a statistically significant difference in the empirical relationship between sail height and keel depths for ridges in the Chukchi/Bering and Beaufort Seas, accounting for positively skewed trends in the data (Gehan, 1965). Separate regressions must be calculated for ridges in the Chukchi/Bering and Beaufort Sea regions.

The measured sail height and keel depths are plotted on Figure 3 for each of the Chukchi and Beaufort regions, along with the linear regression and the 95% confidence interval to represent the range of possible depths for each ridge. After removing two ridges that were outliers, we found a linear regression yielded the best explanatory power. Chukchi ridges are described by H_k = 3.37H_s + 0.47 with an R^2 value of 0.72, while ridges in the Beaufort Sea follow H_k = 3.49H_s + 2.07 with an R^2 value of 0.60 (Figure 3). For the same sail heights, keels in the Beaufort tend to be slightly deeper. We use the 95% confidence interval to provide the upper and lower bands about the keel depth estimate.

3.3 Ridge detection

We apply three criteria to identify grounded ridges: 1) the sails must be at least 0.7 m tall to distinguish from ice floe deformation, 2) sails obey the Rayleigh criteria which distinguishes individual ridges by requiring that the ridge surface descend at least 50% towards the minima on either side of the peak of the sail, and 3) the bathymetric contour must intersect the keel below the undeformed ice draft. Figure 4 shows two ridges (A and B) that are potentially grounded, although one of which

https://doi.org/10.5194/egusphere-2024-1885
Preprint. Discussion started: 1 July 2024

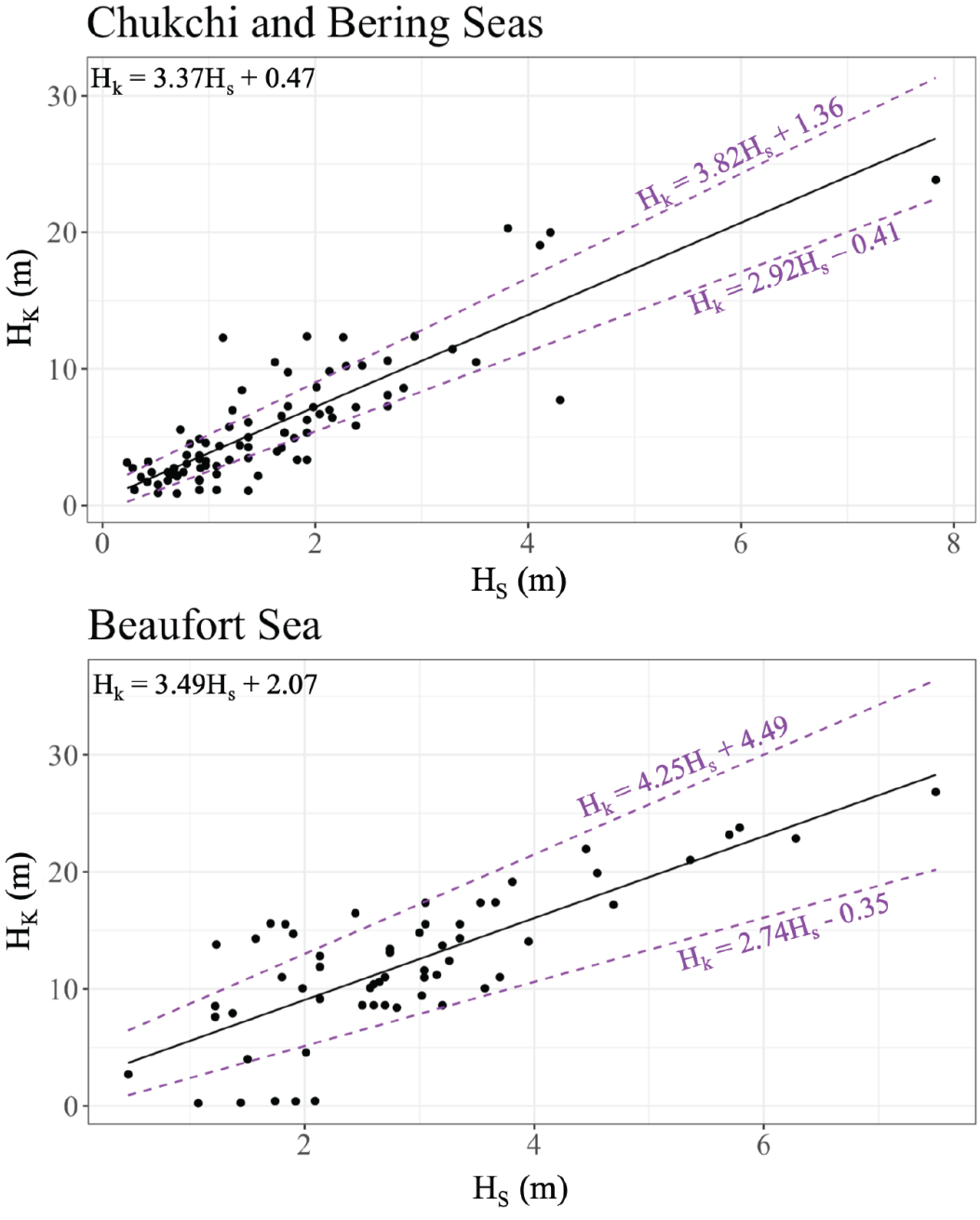

Figure 3. Sail heights (H_s) and keel depths (H_k) from surveyed ridge data (Strub-Klein and Sudom, 2012) in the Chukchi/Bering Seas and the Beaufort Sea with the linear regression equation (black) and 95% confidence intervals (purple) plotted.

(ridge A) intersects the bathymetric line at a depth shallower than the estimated undeformed ice draft. While the ridge is located roughly 400 m from shore, we cannot use the criteria to determine whether this is, in fact, a grounded ridge or whether it is ice

https://doi.org/10.5194/egusphere-2024-1885
Preprint. Discussion started: 1 July 2024

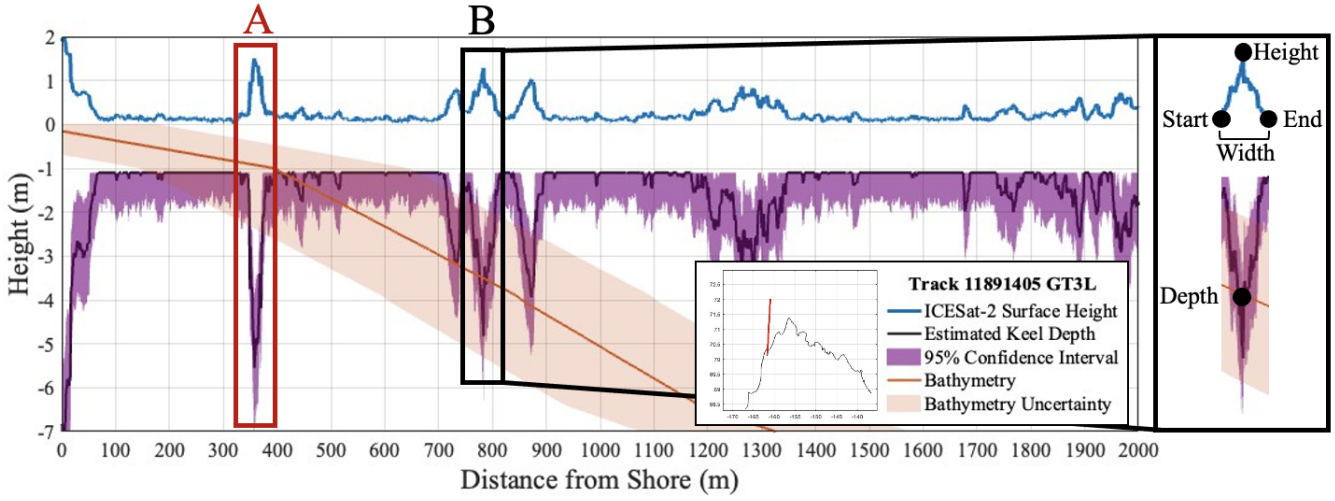

Figure 4. Segment of ICESat-2 surface height (blue) across the sea ice in the Chukchi Sea (map inset) on March 10, 2022 with estimated keel depth (black/purple) and bathymetric depth (orange). Feature A is likely rubble on top of groundfast ice, but feature B is a grounded ridge with estimated keel depths (purple) intersecting the bathymetry (orange). The right side panel shows how we characterized ridge geometry for comparison across the region.

rubble near the shoreline. Ridge B, however, is clearly a grounded ridge where the water depth surrounding the keel exceeds the thickness of the undeformed ice bottom and the estimated keel depth extends deeper than the local bathymetry estimate (orange line). The orange shading represents positional uncertainty in the bathymetry line.

We then record several characteristics of the identified grounded ridges. The right panel of Figure 4 shows how we characterize each grounded ridge feature: the start and end of the ridge in the horizontal direction is used to calculate width, height of the sail, and depth of the bathymetric contour where it intersects the keel depth estimate. In cases where the bathymetric depth changes over the width of the keel, we defined the depth as halfway between the depths at the shoreward and the seaward sides of the keel.

An empirical relationship between maximum sail height and maximum keel depth only applies to ridges and does not estimate the underside of undeformed sea ice. We have applied the FDD modeled ice thickness estimate to undeformed ice so that the figures in this paper show only estimated deformation that extends deeper than the thermodynamic growth. We also neglect ridge width (and especially the width of the keels) as the maximum depth is what matters for this analysis. It is important to note that the estimated keel depth are not meant to be an accurate profile of the under side of the landfast ice.

4 Results

We apply this approach first to three pairs of repeat tracks in the pilot study areas to show the detection of persistent grounded rides, the formation of new grounded ridges during a season, and how the characteristic ridge geometries differ between the

https://doi.org/10.5194/egusphere-2024-1885
Preprint. Discussion started: 1 July 2024

Chukchi and Beaufort sides of the Alaskan coast. We then apply the ridge detection methodology to the entire northern Alaskan coastline for a broader study of ridge characteristics.

4.1 Detection of persistent grounded ridges

Figure 5 shows the surface height of the ice from ICESat-2 using the UMD-RDA along ground track 0373 in the Chukchi Sea (blue) and the GEBCO interpolated bathymetric depth (orange). Estimated keel depths are shown in the purple bands; the keel depth estimate based on the best linear fit of the surveyed ridges is labeled in black and the purple shading shows the 95% confidence interval on the relationship between sail height and keel depth. Using these depth estimations, we identified one ridge that intersects with the sea floor between 0.75 km and 0.85 km from shore. This feature persists from the January 15 track through the April 16 track. Based on the keel estimate and the persistence of the feature, this seems very likely to be a grounded ridge.

Since the altimetric surface height profile suggest that this ridge sail is $\sim$100 m wide, we expect that it is a combination of rubble from the collision(s) that formed the ridge, drifted snow, and possibly the remains of a rafted ice floe. This width is consistent with those reported in Mahoney et al. (2007a). The ICESat-2 track passes roughly perpendicular to shore in this area, and it appears from a time series of Sentinel-1 SAR imagery (Figure 5, lower panels) that the ridged feature near 1 km from shore is approximately perpendicular to the altimetry track. The feature in the SAR imagery appears to be on the order of 50-200 m wide in the off-shore direction and more than a kilometer long in the along-shore direction.

We note that surface features shore-ward of this grounded ridge in Figure 5 remain largely unchanged between the tracks, indicating that the landfast ice is stable over this 91 day period. Surface topography on the seaward side differs more between the two tracks. This is also apparent in the SAR imagery where a new seaward landfast ice edge (SLIE) is established between March 14 and March 26th.

In the SAR imagery, we note persistent features in the ice around the ICESat-2 track that form between December 2 and December 14 last until the end of June. Because these features, including the dark band that is slightly shoreward of the grounded ridge, remain unchanged throughout the season, we can infer the stability of the ice and confirm the presence of grounded ridges in the area.

4.2 Feature persistence and detection of new grounded ridges

The period from January to April between repeat tracks is more than long enough for the development of new grounded ridges. Figure 6 shows a series of five ridge features between 0.65 km and 1.45 km off shore that are likely grounded from January 15 through the April 16 ICESat-2 tracks. The April 16 track includes an additional ridge feature from 1.85-2 km off shore that is also likely to be grounded.

The set of five ridge features present in both tracks may not all be deep enough to be grounded: the best estimate for keel depth for Chukchi ridges comes to within a meter of the bathymetry for the more seaward ridges (starting from the 2 label outward) but does not intersect the bathymetric line. As these are among the most seaward features in the January track, they would be susceptible to breaking off if not anchored by a grounded ridge. However, the persistence of these features between

https://doi.org/10.5194/egusphere-2024-1885
Preprint. Discussion started: 1 July 2024

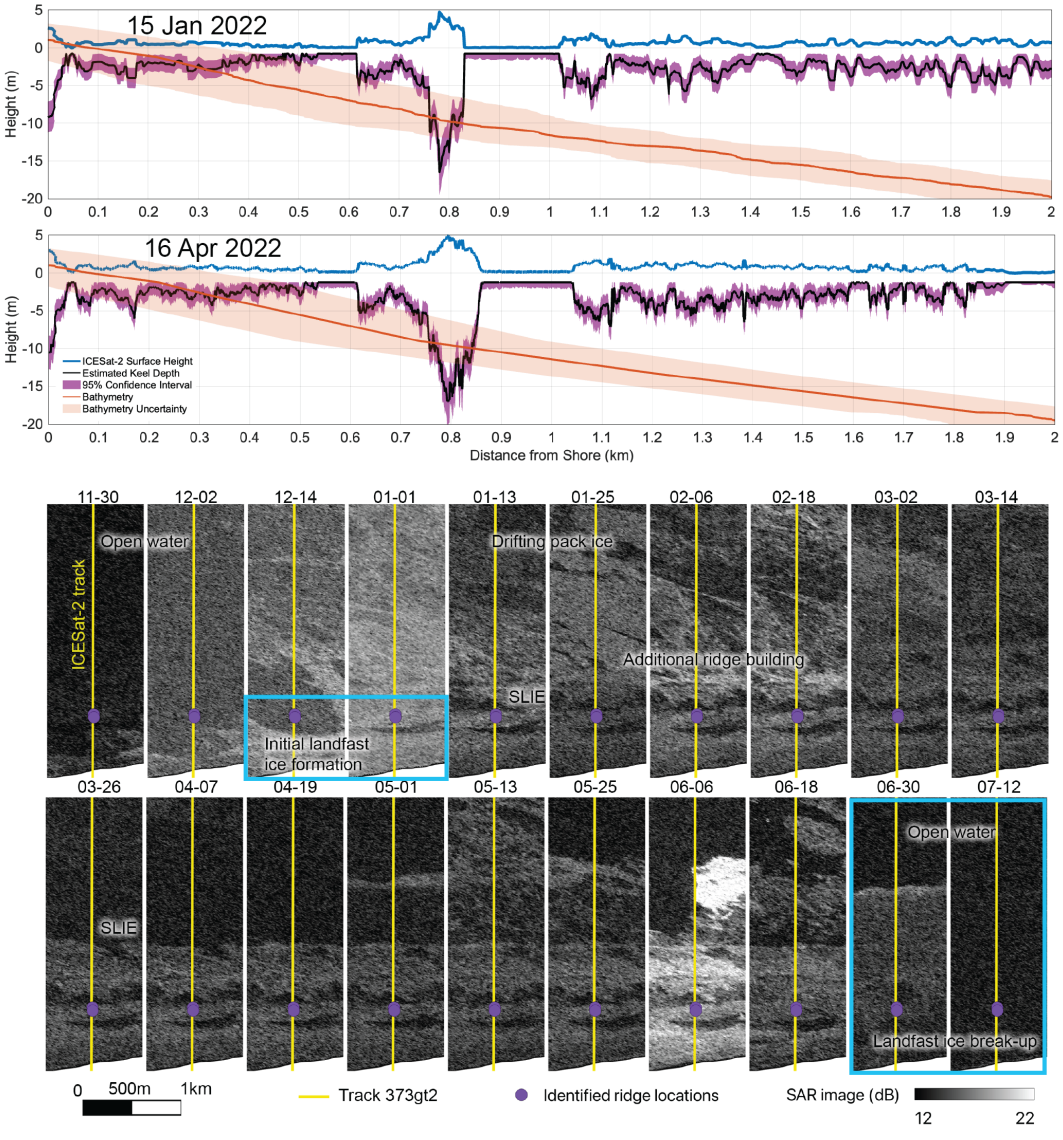

Figure 5. Top: Paired ridge profiles from ICESat-2 tracks 0373 GT2L (blue) in the Chukchi pilot study area to the west of Point Barrow (71.19° N, 157.04° W) on 15 January and 16 April 2022. We find a likely grounded ridge at ∼0.8 km off shore, based on keel depth estimates (black line, purple shading) intersecting the bathymetry (orange). Bottom: Sentinel-1 SAR backscatter images surrounding the ICESat-2 track (0373 GT2L, indicated by the yellow line) with the grounded ridge indicated by a purple dot. Panels outlined in blue denote the periods of formation and breakup of persistent features in the sea ice.

the two tracks suggests stability. The last of the ridges in this series might be sufficient to hold these features in place, or this ice may be connected laterally to grounded ridge segments elsewhere.

https://doi.org/10.5194/egusphere-2024-1885
Preprint. Discussion started: 1 July 2024

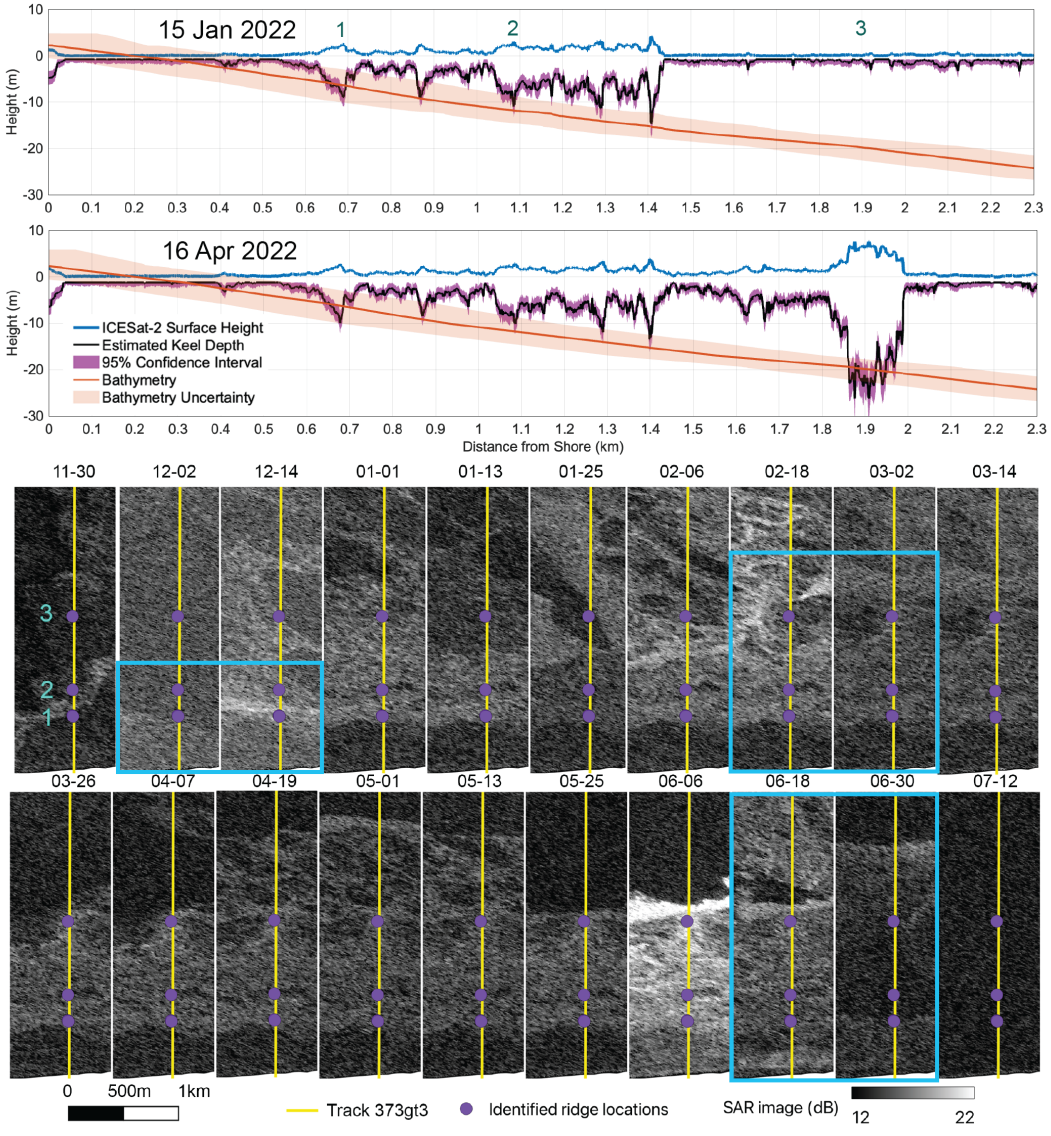

Figure 6. Top: Paired ridge profiles from ICESat-2 tracks 0373 GT3L (blue) in the Chukchi pilot study area to the west of Point Barrow (71.23° N, 156.96° W) on 15 January and 16 April 2022. We find a series of five possibly grounded ridges ∼0.7, 0.85, 1.1, 1.3, and 1.4 km off shore, based on keel depth estimates (black line, purple shading) intersecting the bathymetry (orange). An additional large grounded ridge is formed sometime after the January 15 ICESat-2 track. Three ridges are labeled with numbers in both panels for comparison. Bottom: Sentinel-1 SAR backscatter images surrounding the ICESat-2 track (0373 GT3L, indicated by the yellow line) with the grounded ridge indicated by a purple dot. Panels outlined in blue denote the periods of formation and breakup of persistent features in the sea ice.

In the April track, there are slight changes in the best estimate keel depths. This is not likely due to a change in the surface height of the features themselves, but rather that snow accumulation and redistribution has increased the detected surface

https://doi.org/10.5194/egusphere-2024-1885
Preprint. Discussion started: 1 July 2024

height of the flat, undeformed ice surface relative to the ridges. The ridge peaks in the April tracks are slightly higher relative to the estimated water level than in the January tracks because the water level is calculated from the buoyant equilibrium of thermodynamically grown ice thickness estimated with the FDD model.

Between the January and April tracks, a new grounded ridge feature (labeled 3) appears between 1.8-2 km from shore. In the SAR imagery, there are persistent features near where we identify that ridge that form in late February and last through the May 13 image. They are not the classic linear, roughly parallel to shore shape common for ridges in coastal ice, but the prevalence of shear deformation on the Chukchi side of Point Barrow is known to form ridges at a range of angles relative to shore. The spatial resolution of the SAR imagery poses a challenge for unambiguous interpretation of grounded ridges and is an insufficient tool by itself for determining where exactly ridge features form or for characterizing their geometry. The ICESat-2 profile of the ridge shows that the horizontal scale of the feature is $\sim$ 200 m wide and the sail extends $\sim$5 m above the surface with a keel reaching approximately 20 m deep. This depth is consistent with the stamuki zone ($\geq$ 10 m) where grounded ridges are often found.

4.3 Comparison of Chukchi and Beaufort ridge detections

Figure 7 applies the same approach as used in Sections4.1 and 4.2 to shorefast ice on the Beaufort side of Point Barrow, using the empirical relationship between sail height and keel depth derived for the Beaufort region. Here, we find that the likely grounded ridges are located farther from shore than the data examined in the Chukchi Sea, consistent with a wider band of landfast ice (Cooley and Ryan, 2024; Mahoney et al., 2014). This is a result of the shallower sea floor extending farther from shore along the coastline of the Beaufort Sea, as well as a different ice motion regime relative to the shoreline (Zhao and Liu, 2007). The patterns in ridges persist between the January and April tracks indicate the stable shorefast ice likely extends to at least 6 km, and up to 13 km, from shore.

Our examples illustrate that the ice surface in the Beaufort Sea study area is notably more deformed than the Chukchi Sea study area, with smaller ridges (<2 m sail height and <50 m width) occurring roughly every 200 m. In this profile, there are not larger ridges ($\sim$5 m sail height), which we found in the two Chukchi-side tracks.

We note several persistent features in this track, but do not identify any as certainly grounded. The near-shore section may have 1–2 km of bottomfast ice in the shallow (<4 m) water near the spit separating Elson Lagoon from the Beaufort Sea. We note one feature with significant deformation around 3.5–4.2 km from shore (see inset) that persists between the January and April tracks but does not necessarily intersect the bathymetry line. Further features out to 12km from shore are highly similar between the two tracks, and the SAR imagery suggests little ice movement between January 1 and June 6. We suggest, based on the stability of the ice over the 91 day period, that this region of shorefast ice may be laterally grounded.

4.4 Ridge characterization and mapping

Applying this algorithm across the entire Alaskan Arctic, we measure 490 individual grounded ridges in the Chukchi Sea along ICESat-2 tracks, and 803 along the Beaufort coastline. We compile a database of parameters for each ridge including height, depth, width, and distance from shore for each ridge, and the number of ridges per ICESat-2 track. We also calculate

https://doi.org/10.5194/egusphere-2024-1885
Preprint. Discussion started: 1 July 2024

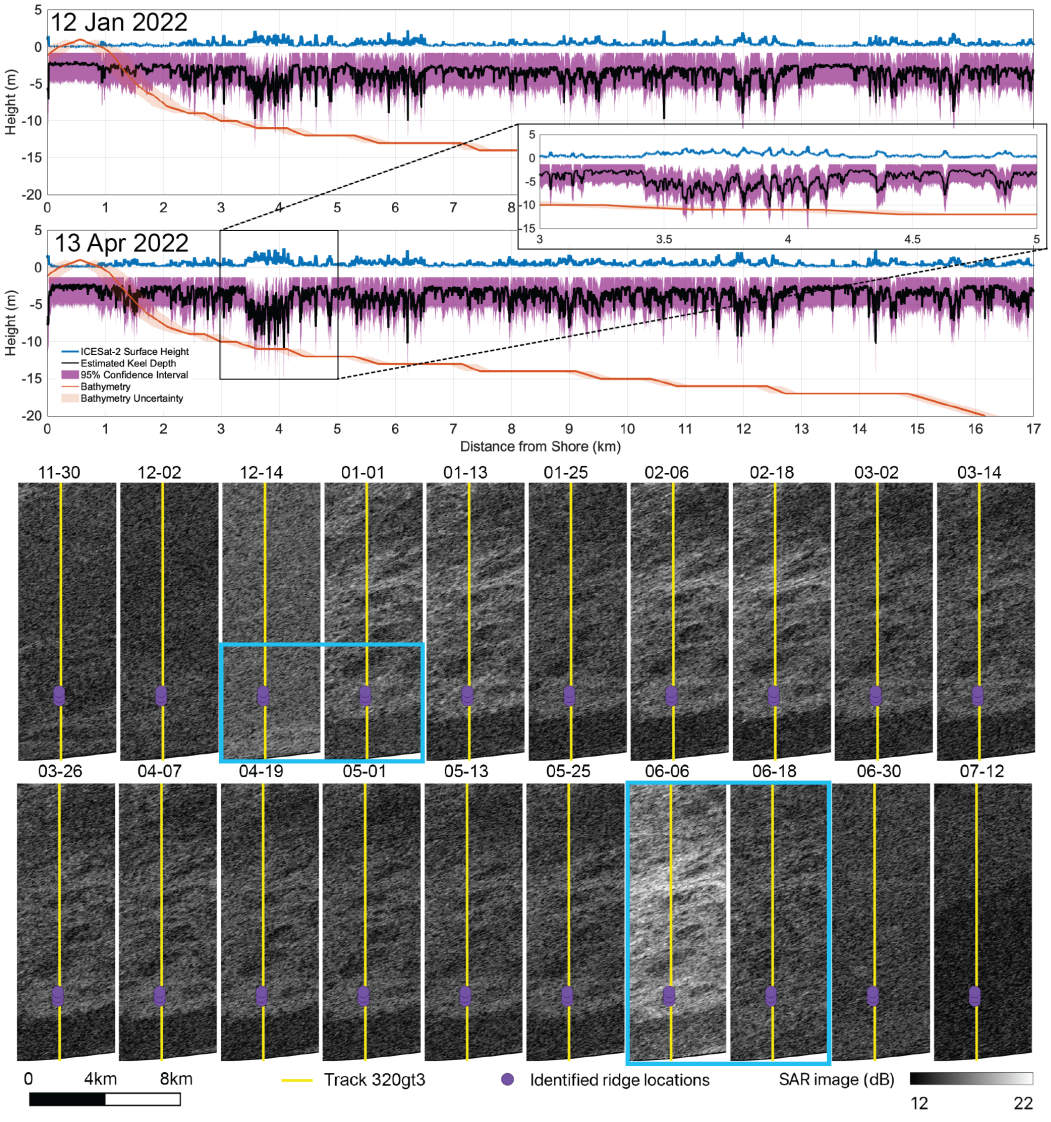

Figure 7. Top: Paired ridge profiles from ICESat-2 tracks 0373 GT3L (blue) in the Beaufort Sea to the east of Point Barrow (71.32° N, 155.99° W) on 12 January and 13 April 2022. We find an area with possibly grounded ridges between 3.5-4 km off shore, based on keel depth estimates (black line, purple shading) intersecting the bathymetry (orange) that is magnified in the inset. Bottom: Sentinel-1 SAR backscatter images surrounding the ICESat-2 track (0320 GT3L, indicated by the yellow line) with detected grounded ridges indicated by purple dots. Panels outlined in blue denote the periods of formation and breakup of persistent features in the sea ice.

the location of each ridge relative to the landfast ice edge as detected by Cooley and Ryan (2024), recording it as a percentage between the SLIE and coastline (Equation 4).

https://doi.org/10.5194/egusphere-2024-1885
Preprint. Discussion started: 1 July 2024

Region	Metric	Mean	Min	Median	Max	stdev
Chukchi	Depth	5.5 m	0.8 m	4.3 m	19.9 m	3.5 m
	Ridges/Track	2.0	0	2.0	9	1.93
	Distance	1.8 km	220 m	990 m	26.6 km	2.6 km
	Height	2.0 m	0.6 m	1.7 m	7.6 m	1.1 m
	Width	57.0 m	1.9 m	40.2 m	813.7 m	64.3 m
	Percent out from coast	22.3%	2.1%	13.5%	96.2%	20.2%
Beaufort	Depth	9.2 m	1.7 m	8.0 m	29.0 m	4.5 m
	Ridges/Track	1.87	0	1.0	11	1.95
	Distance	10.7 km	186.1 m	7.5 km	72.6 km	9.5 km
	Height	2.6 m	0.7 m	2.0 m	7.4 m	1.2 m
	Width	123.9 m	3.0 m	89.3 m	1552 m	122.1 m
	Percent out from coast	28.4%	0.2%	20.4%	96.5%	22.4%

Table 2. A summary of calculated grounded ridge metrics from the Chukchi and the Beaufort Seas from December 1, 2021 - May 1, 2022. The full list of grounded ridges with their dimensions is provided in the supplemental material.

$$\begin{matrix}\text{percent out}\\ \text{from coast}\end{matrix} = \left(\frac{\text{distance to coast}}{\text{distance to coast} + \text{distance to SLIE}}\right) \times 100\% \tag{4}$$

The statistics (Table 2) reveal several notable differences between ridges in the Chukchi and Beaufort regions. Most significantly, the grounded ridges in the Beaufort are located on average 8.94 km farther from the shoreline than the grounded ridges in the Chukchi Sea. We also find that grounded ridges in the Beaufort Sea tend to be wider, deeper, and taller than those in the Chukchi Sea, while the number of grounded features per track is comparable between the two locations.

Our data shows mean depths of 5.5 $\pm$ 3.5 m in the Chukchi and 9.2 $\pm$ 4.5 m in the Beaufort regions, with only 10.2% of grounded ridges in the Chukchi side and 32.8% in the Beaufort side of Arctic Alaska falling within the stamuki zone ($\geq$ 10 m bathymetric depth). Our results indicate that ridges ground the sea ice at all bathymetric depths between the landfast ice edge and the shoreline, with a majority occurring in shallower water. Even if we only consider the furthest seaward ridge along each track, the average depth is still only 7.2 m and 11.2 m in the Chukchi and Beaufort regions respectively. This disconnect between the traditional definition of the grounding zone along coastlines and our results indicates one of a few things: climatic changes and a warming Arctic are causing grounded ridges to form at shallower depths, more shoreward grounded ridges have been ignored, and/or the bathymetric data is incorrect.

Mahoney et al. (2007a) assumes a sail width of 100 m for grounded ridges. Our analysis shows average sail widths of 57 and 124 m for Chukchi and Beaufort grounded ridges, respectively. This difference could be due to ICESat-2 tracks measuring ridges at an angle that is not perpendicular to the ridge axis, but we mitigate this concern by calculating the distance from shore rather than distance along track for each individual ICESat-2 surface height measurement. This approach allows us to correct

https://doi.org/10.5194/egusphere-2024-1885
Preprint. Discussion started: 1 July 2024

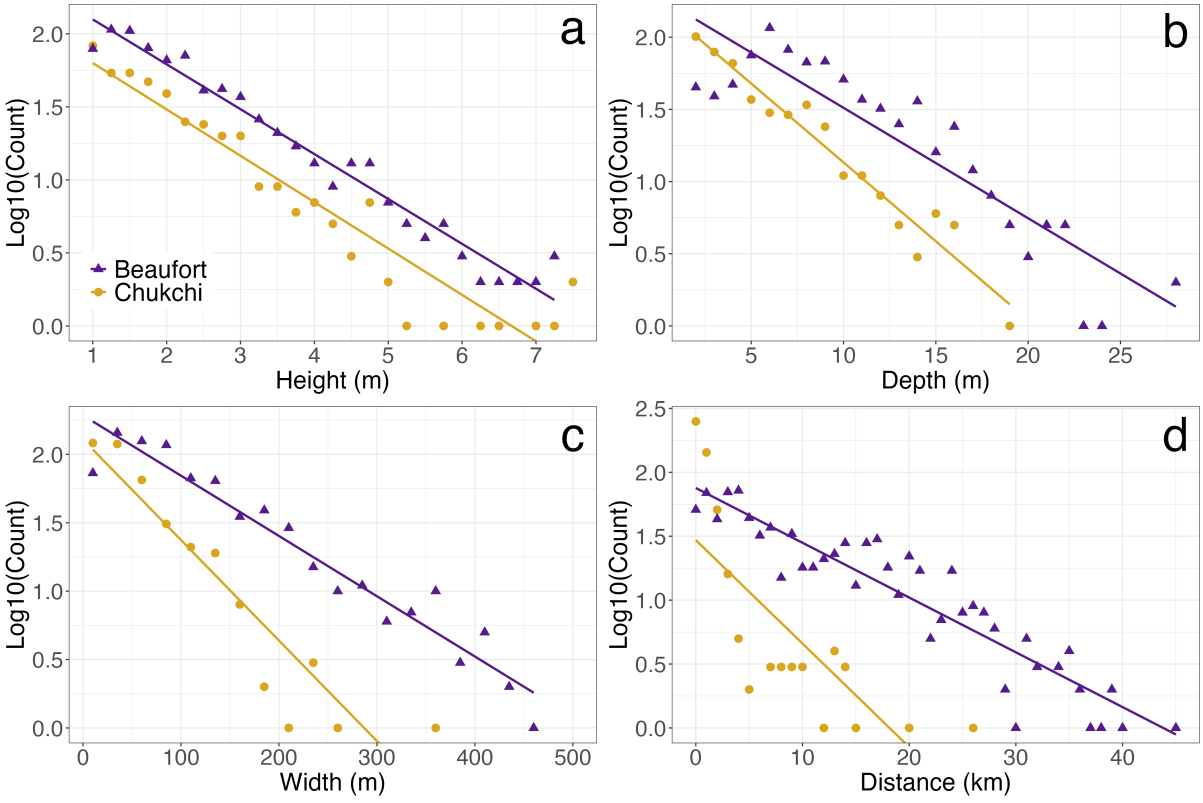

Figure 8. Log histogram plots of grounded ridge (a) sail height, (b) bathymetric depth, (c) width, and (d) distance from shore, with solid lines indicating an exponential fit to the data. Heights are binned at 0.25 m, depths by 1 m, width by 25 m, and distance from shore by 1 km.

for angular distortions and collect more accurate width data, to the extent that ridges in shorefast ice are generally roughly parallel to the shoreline. A field campaign would be necessary to compare ICESat-2 surface height profiles and estimated keel depths with under-ice measurements in order to fully validate our ridge profiles.

Mahoney et al. (2007a) suggested grounded ridges discontinuously pin the landfast ice edge, roughly every 30 km. However, field observations by Mahoney (2006) suggest the spacing between these ridges may be closer, a notion supported by our results. We find, on average, 2.0 ridges per ICESat-2 ground track in the Chukchi region and 1.9 per track in the Beaufort region. Given these tracks pass over an effectively random sampling of coastal Arctic sea ice, and that there are on average >1 ridge per track, we can infer that any location is likely grounded by at least one ridge, though there are certainly some places without any grounded ridges (15% of ICESat-2 surface height profiles examined contained no grounded ridges). Additionally, Mahoney et al. (2007a) assumes that these grounded ridge features are located close to the SLIE, and while we find this to be true in some cases, the average location of ridges were located just 22.3% and 28.4% away from the coastline in the Chukchi and Beaufort Sea regions, respectively. Together, this suggests that coastal sea ice is regularly pinned by frequent grounded ridges in the shallow water (< 10 m depth) and infrequent grounded ridges in the deeper stamuki zone.

https://doi.org/10.5194/egusphere-2024-1885
Preprint. Discussion started: 1 July 2024

Next, we examine height, depth, distance from shore, and width to understand how grounded ridge geometries vary between the two regions. Figure 8 shows log histogram plots comparing the grounded ridge measurements. Since the total number of ridges differs between the two regions, the count of grounded ridges in the Beaufort Sea is consistently larger than that of the Chukchi Sea. Exponential fits to the histograms of grounded ridge height in the Beaufort and Chukchi regions are parallel (Figure 8a), indicating similar distributions between the two regions. The distribution of depths follows a similar result between the two regions with a slight preference towards shallower sea floor depths in Chukchi grounded ridges (Figure 8b). We find a tendency towards narrower ridge widths in the Chukchi region compared to ridges in the Beaufort (Figure 8c). Grounded ridges in the Chukchi tend to form closer to shore than in the Beaufort (Figure 8d).

We find a strong positive relationship between height and bathymetric depth, as increasing bathymetric depths correspond to greater sail heights. This is expected: the maximum estimated depth of a ridge is a linear function of the sail height and grounded ridges occur when ridge depth exceeds bathymetric depth. The minimum bathymetric depth of a grounded ridge is, by definition, a linear function of sail height. In the Beaufort Sea, grounded ridges at the same bathymetric depth tend to be slightly taller than those in the Chukchi region, which is likely a result of the different shoreline aspect relative to the predominant ice drift direction or differences in thickness of the parent ice floe.

Next, we consider seasonal trends in height, depth, distance from shore, and width. We plot means of grounded ridge properties over two week periods throughout the winter on Figure 9 and find that height (a), depth (b), width (c), and distance from shore (d) tend to increase until March or April. In the Chukchi Sea region, the mean sail height of grounded ridges more than doubles during the winter season, from 0.9 m in Dec 2021 to 2.4 m by the end of March 2022. While height increased in the Beaufort Sea region with time, there was a slower growth starting at 1.8 m in December and reaching 2.7m towards the end of February. The bathymetric depths of grounded ridges in the Chukchi and Beaufort regions increased similarly over the season, from 2.2 m in December to 7.1 m in mid-March, and from 4.2 m in December to 11.2 m in end of February respectively, forming at shallower depths in the Chukchi Sea. Width increases from 40 m and 60 m in December to 100 m and 127 in February and March, with most of the increase happening before mid-January.

Mean distance from shore increased as well, starting around 1 km from shore in the Chukchi and 5.7 km in the Beaufort in December and ending as high as 2.8 km in April (Chukchi) and 12.5 km in March (Beaufort). Seasonal trends in distance from shore are complicated by the fact that each track contains ridges formed at any time up to that point the season: a March track might include near-shore ridges formed in January. We interpret these seasonal increases as evidence that ridges form further from shore and at greater depths as shore ice stabilizes and that ridges may be built up by subsequent collisions causing them to increase in size over the season. The latter would suggest an increase in width over the season: given that the increases in ridge width are primarily found early in the season, it seems likely that for most of the winter changes in distance from shore are due to the formation of new ridges further from shore (e.g., Section 4.2).

Figure 10 maps grounded ridge locations. Extended linear features form roughly parallel to the shoreline, as we would expect from the predominant pack ice drift direction being towards the southwest in the southern Beaufort Sea. Notably, one distinct feature spans approximately 150 km between -146 and -150°W, roughly parallel to the shoreline. While ICESat-2 data alone

https://doi.org/10.5194/egusphere-2024-1885
Preprint. Discussion started: 1 July 2024

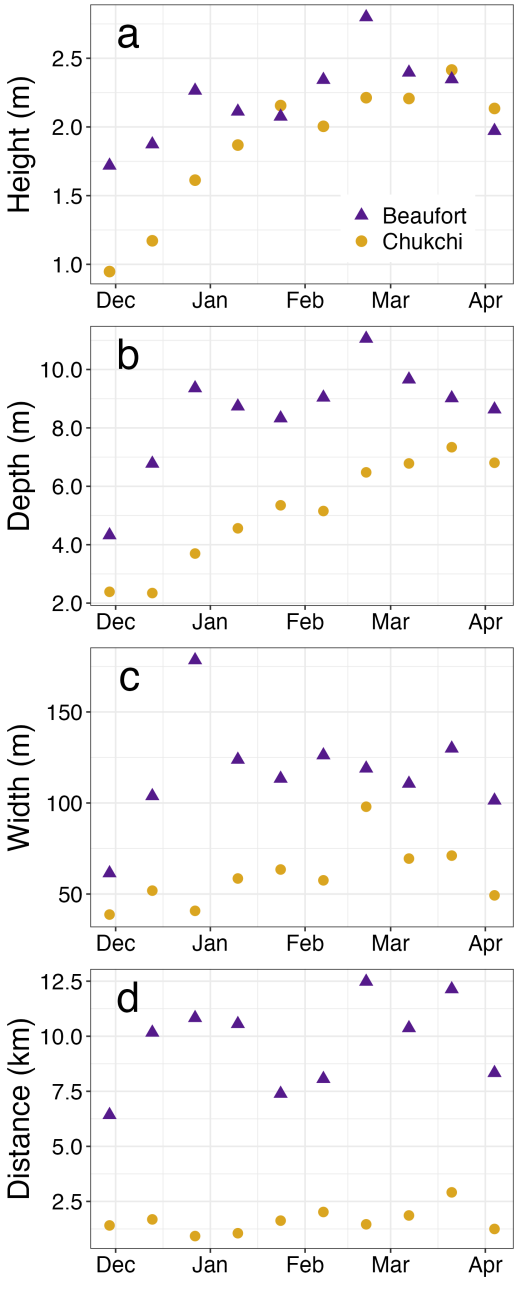

Figure 9. Seasonal evolution of grounded ridge (a) sail height, (b) bathymetric depth, (c) width, and (d) distance from shore between 1 Dec 2021 and 1 May 2022. Data were aggregated over 2-week periods, with each period including a number of ridges ranging from 12 to 90 in the Chukchi Sea and 19 to 56 in the Beaufort Sea.

https://doi.org/10.5194/egusphere-2024-1885
Preprint. Discussion started: 1 July 2024

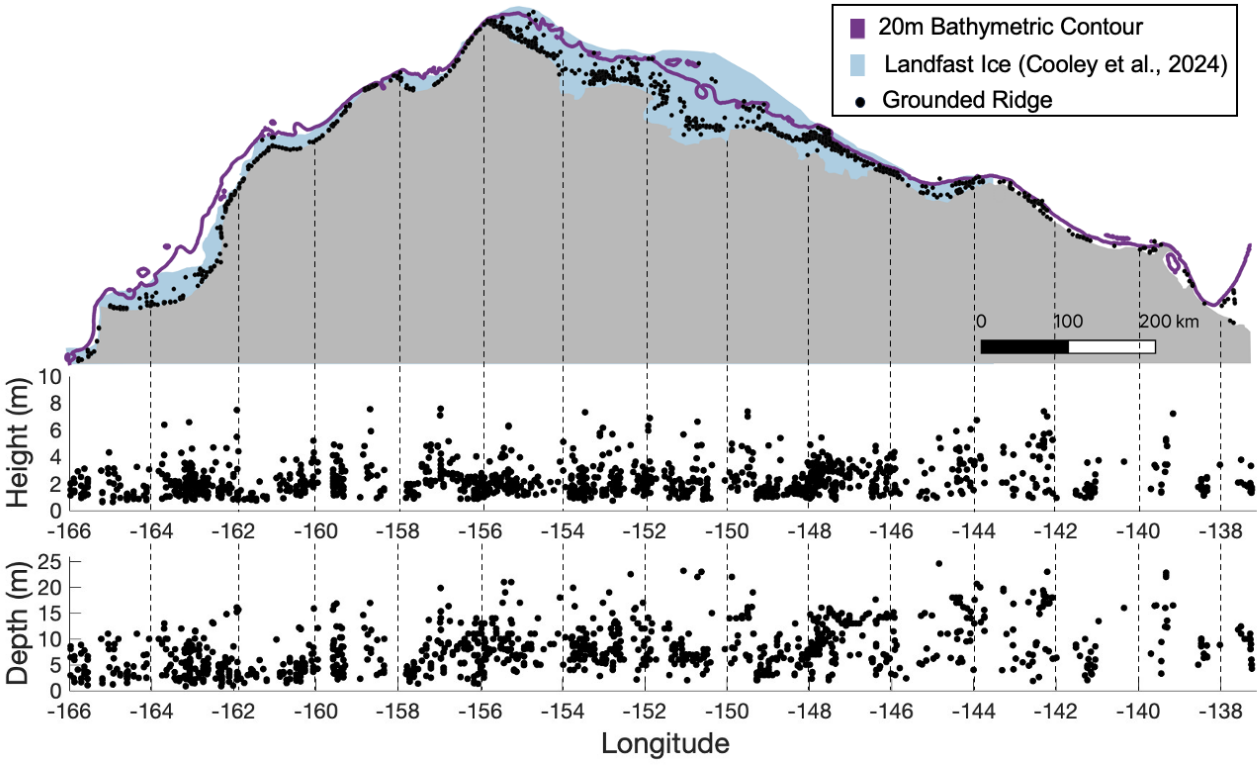

Figure 10. Grounded ridges detected in ICESat-2 tracks (black) along the Alaskan Coastline between December 1, 2021 and May 1, 2022. The blue shading represents the landfast ice extent as published by Cooley and Ryan (2024) and the purple line tracks the 20 m bathymetric contour (GEBCO Compilation Group, 2023).

cannot determine whether these are extensions of the same grounded ridge or separate shorter ridge segments, it nevertheless broadens our understanding of conditions and locations in which grounded ridges tend to form.

Along the Chukchi coast, ridges are located close to the shore, with a mean distance of 1.76 km off shore. In contrast, along Beaufort Sea coastline, grounded ridges are generally located much farther from shore, with a mean distance of 10.69 km. All of the grounded ridges detected in this study fall within the bounds of the independently-estimated landfast ice edge for the 2021-2022 winter (blue, which is only shown west of 143° W due to the available data from Cooley and Ryan (2024)). Additionally, most of the ridges are located in water shallower than the 20 m isobath, with a few extending slightly deeper around 151° W.

We also plot the height and depth of ridges across this coastline (Figure 10, lower panels), finding that patterns in regional variability across the coastline are difficult to distinguish. The overall statistics indicate that ridges form at slightly deeper locations in the Beaufort region compared to the Chukchi, but there is significant variability in ridge height and distance from shore in both areas. Relatively few ridges fall at depths greater than the 15 m isobath on either side of the coast.

https://doi.org/10.5194/egusphere-2024-1885
Preprint. Discussion started: 1 July 2024

There are a few notable gaps in the data, including around longitudes 159° W, 142° W, and 139° W. These are gaps in ICESat-2 coverage, likely due to adverse weather on one or both of the two passes in these locations over the winter season.

4.5 Limitations of this approach

There remains some uncertainty around the role of relatively flat, undeformed ice in some of the assumptions underlying our analysis. Sail heights are measured relative to the surface of the surrounding undeformed ice, but the calculation of keel depth is based on the height of the sail relative to the water line. Thermodynamic ice growth over the course of the winter season will slightly change the water line relative to ridge peaks and accordingly change the estimate of the sail height (H_s) that we use to calculate the keel depth. If the change in thermodynamic ice thickness was very large, we would expect repeat tracks to show artificial growth of the ridge keels over the winter season, which none of the profiles above show.

There is also some uncertainty associated with the bathymetric data used in our study: sediment transport, ice scouring, and limitations of measuring depths close to the coast in icy waters all mean that the bathymetric data represents an approximation of the depth of the sea floor. For ridges where the whole 95% confidence interval (indicated by the purple shading) intersects the sea floor, and the features remain persistent between two dates, we can detect grounded ridges with some certainty. The 500 m resolution of the GEBCO bathymetric product is also highlighted on the Figures 5, 6, and 7 to better understand the spatial uncertainty associated with a coarse product.

Our analysis of ICESat-2 repeat-track data throughout winter 2021–2022 suggests that the repeat alignment of the ground tracks in this area is accurate to 10-20 m. This is within the mission requirements (Markus et al., 2017) and consistent with the ICESat-2 footprint size of $\sim$11 m (Magruder et al., 2024). However, given the small-scale variability of sea ice ridges and rubble, small changes in ground-track geolocation between repeat passes could result in differences in pressure ridge height and width. Analyzing the difference in surface height between pairs repeat tracks did not yield notable results and could be explained by snow redistribution or subsequent collisions causing ridges to shift slightly.

Over level ice surfaces, such as refrozen leads, ICESat-2 surface heights have a precision of 1-2 cm (Kwok et al., 2019; Farrell et al., 2020). Through comparisons with independent airborne measurements, Ricker et al. (2023) and Farrell et al. (2020) have also demonstrated that, on average, ridge sail heights measured using the UMD-RDA algorithm are accurate to $\sim$0.1 m.

Finally, it is possible some of the features which we record as grounded are not actually ridges in the sea ice. Oil rigs are a known infrastructural feature prevalent offshore from the Alaskan coastline, as part of the National Petroleum Reserve. They are likely to be present in some of the ICESat-2 tracks, and due to the resolution of the altimetry product, and the size of the rigs, we suspect they could appear similar to a ridge without further context. Frequent spring fog in the region (Khalilian, 2016) may also cause erroneous surface elevation measurements resulting from reflected photons which are not captured by the filters in the data processing algorithm.

https://doi.org/10.5194/egusphere-2024-1885
Preprint. Discussion started: 1 July 2024

5 Conclusions

Using available data from ICESat-2, Sentinel-1, and GEBCO bathymetric products, we present a methodology to identify grounded sea ice ridges over the course of a winter season. This approach can be applied to coastal regions throughout the Arctic, wherever there is a need for monitoring the development of grounded ridges. This process can be combined with additional data products (e.g., high-resolution radar or SAR imagery) to confirm the stability of surrounding ice features. Comparing surface heights from ICESat-2 repeat tracks in the Chukchi and Beaufort Seas, we could confirm that particular ridges were grounded and stabilizing the surrounding ice. For communities with either infrastructure to support a sea ice radar system (e.g., Utqiaġvik, (UAF, 2022)) or with active community observers (e.g., Alaska Arctic Observatory and Knowledge Hub database (Adams and Observers of coastal Arctic Alaska, 2022)), these surface-based observations could be used instead of or in addition to the SAR imagery for constraining ridge development in time. While underlying uncertainties in bathymetric data exist, these can be addressed with additional bathymetric surveys in near-shore environments.

These findings are significant for a number of reasons: grounded ridges impact coastal community subsistence hunting, transportation, and safety, provide habitat for animals, and stabilize the coastline from erosion. In the face of warming temperatures and the uncertainties of climate change, our approach may serve as a critical tool for ongoing monitoring and understanding of shorefast ice stability and seasonality. As we accumulate a longer ICESat-2 dataset, this approach may be used to track changes in shorefast ice timing and grounded ridge formation over time.

To continue improving on our approach and addressing some of the known limitations, in situ surveys of ridge morphology in the near-shore environment are needed to further validate this process. We rely on statistics of ridge geometry in off-shore environments to estimate keel depths, which may not necessarily apply to shorefast ice. Additional bathymetric surveys are necessary to constrain uncertainties associated with sea floor depth estimates.

A wider application of this approach to shorefast ice observation could be used to validate modeling efforts at capturing landfast ice dynamics (e.g., (Lemieux et al., 2015)). Modern models are incapable of reflecting seasonal landfast ice variability which impacts sea ice thickness and concentration results, halocline stability (Itkin et al., 2015), upwelling estimations (Kasper and Weingartner, 2015), and brine expulsion (Selyuzhenok et al., 2015). Shorefast ice also blocks momentum flux between the atmosphere and ocean, isolating the ocean from wind-driven mixing and limiting upwelling, and causes river plumes to extend to further distances under the ice (Granskog et al., 2005). While the process of grounded ridge formation exist at sub-grid scale in current models, ridges impact larger scale ice movement and near shore dynamics. Ultimately, the approach outlined in this study creates opportunities to observe grounded ridge properties across much larger spatial scales, opening potential avenues for improved understanding of coastal Arctic processes.

Code and data availability. The processing code used for this project is available at https://doi.org/10.5281/zenodo.12518280 . ICESat-2 ATL03 data are publicly available from the National Snow and Ice Data Center (https://nsidc.org/data/atl03/versions/6). The UMD-RDA processed data used in this study is available at https://doi.org/10.5281/zenodo.12188016 .

https://doi.org/10.5194/egusphere-2024-1885
Preprint. Discussion started: 1 July 2024

Author contributions. KL: data analysis, writing, AB: project conception, advising, writing, SLF: ICESat-2 data processing, reviewing of draft/writing, KD: ICESat-2 data processing

Competing interests. No competing interests are present.

Acknowledgements. SLF and KD were supported by NASA Cryosphere Grant 80NSSC20K0966. KL was supported by student research funding through the Williams College Geoscience Department.

https://doi.org/10.5194/egusphere-2024-1885
Preprint. Discussion started: 1 July 2024

References

Adams, B. and Observers of coastal Arctic Alaska: Local Observations from the Seasonal Ice Zone Observing Network (SIZONet) and Alaska Arctic Observatory and Knowledge Hub (AAOKH), Version 2., https://doi.org/https://doi.org/10.7265/jhws-b380, 2022.

Amante, C. J.: Estimating coastal digital elevation model uncertainty, Journal of Coastal Research, 34, 1382–1397, 2018.

Anderson, D. L.: Growth Rate of Sea Ice, Journal of Glaciology, 3, 1170–1172, https://doi.org/10.3189/S0022143000017676, 1961.

Barnes, P. W., Reimnitz, E., and Fox, D.: Ice rafting of fine-grained sediment, a sorting and transport mechanism, Beaufort Sea, Alaska, Journal of Sedimentary Research, 52, 493–502, 1982.

Barnes, P. W., Asbury, J. L., Rearic, D. M., and Ross, C. R.: Ice erosion of a sea-floor knickpoint at the inner edge of the stamukhi zone, Beaufort Sea, Alaska, Marine geology, 76, 207–222, 1987.

Barry, R., Moritz, R. E., and Rogers, J.: The fast ice regimes of the Beaufort and Chukchi Sea coasts, Alaska, Cold Regions Science and Technology, 1, 129–152, 1979.

Baztan, J., Cordier, M., Huctin, J.-M., Zhu, Z., and Vanderlinden, J.-P.: Life on thin ice: Insights from Uummannaq, Greenland for connecting climate science with Arctic communities, Polar Science, 13, 100–108, 2017.

Cooley, S. W. and Ryan, J. C.: Community-scale changes to landfast ice along the coast of Alaska over 2000-2022, Environmental Research Letters, 2024.

Cooley, S. W., Ryan, J. C., Smith, L. C., Horvat, C., Pearson, B., Dale, B., and Lynch, A. H.: Coldest Canadian Arctic communities face greatest reductions in shorefast sea ice, Nature Climate Change, 10, 533–538, 2020.

Dammann, D. O., Eriksson, L. E., Mahoney, A. R., Eicken, H., and Meyer, F. J.: Mapping pan-Arctic landfast sea ice stability using Sentinel-1 interferometry, The Cryosphere, 13, 557–577, 2019.

Druckenmiller, M. L., Eicken, H., George, J. C., and Brower, L.: Assessing the shorefast ice: Iñupiat whaling trails off Barrow, Alaska, SIKU: Knowing Our Ice: Documenting Inuit Sea Ice Knowledge and Use, pp. 203–228, 2010.

Duncan, K. and Farrell, S. L.: Determining variability in Arctic sea ice pressure ridge topography with ICESat-2, Geophysical Research Letters, 49, e2022GL100 272, 2022.

Eicken, H., Lovecraft, A. L., and Druckenmiller, M. L.: Sea-ice system services: A framework to help identify and meet information needs relevant for Arctic observing networks, Arctic, pp. 119–136, 2009.

Farrell, S., Duncan, K., Buckley, E., Richter-Menge, J., and Li, R.: Mapping sea ice surface topography in high fidelity with ICESat-2, Geophysical Research Letters, 47, e2020GL090 708, 2020.

Gearheard, S., Matumeak, W., Angutikjuaq, I., Maslanik, J., Huntington, H. P., Leavitt, J., Kagak, D. M., Tigullaraq, G., and Barry, R. G.: "It's not that simple": a collaborative comparison of sea ice environments, their uses, observed changes, and adaptations in Barrow, Alaska, USA, and Clyde River, Nunavut, Canada, AMBIO: A Journal of the Human Environment, 35, 203–211, 2006.

GEBCO Compilation Group: GEBCO Gridded Bathymetry Data: GEBCO_2023 15 arc-second grid. Subset: 67° to 73° N, 168° to 133° W, https://download.gebco.net/, 2023.

Gehan, E. A.: A generalized Wilcoxon test for comparing arbitrarily singly-censored samples, Biometrika, 52, 203–224, 1965.

George, J. C., Huntington, H. P., Brewster, K., Eicken, H., Norton, D. W., and Glenn, R.: Observations on shorefast ice dynamics in Arctic Alaska and the responses of the Iñupiat hunting community, Arctic, pp. 363–374, 2004.

Gerland, S., Renner, A., Godtliebsen, F., Divine, D., and Løyning, T.: Decrease of sea ice thickness at Hopen, Barents Sea, during 1966–2007, Geophysical Research Letters, 35, 2008.

https://doi.org/10.5194/egusphere-2024-1885
Preprint. Discussion started: 1 July 2024

Granskog, M. A., Ehn, J., and Niemelä, M.: Characteristics and potential impacts of under-ice river plumes in the seasonally ice-covered Bothnian Bay (Baltic Sea), Journal of Marine Systems, 53, 187–196, 2005.

Hošeková, L., Eidam, E., Panteleev, G., Rainville, L., Rogers, W. E., and Thomson, J.: Landfast ice and coastal wave exposure in northern Alaska, Geophysical Research Letters, 48, e2021GL095 103, 2021.

Howell, S. E., Laliberté, F., Kwok, R., Derksen, C., and King, J.: Landfast ice thickness in the Canadian Arctic Archipelago from observations and models, The Cryosphere, 10, 1463–1475, 2016.

Huntington, H. P., Zagorsky, A., Kaltenborn, B. P., Shin, H. C., Dawson, J., Lukin, M., Dahl, P. E., Guo, P., and Thomas, D. N.: Societal implications of a changing Arctic Ocean, Ambio, 51, 298–306, 2022.

Itkin, P., Losch, M., and Gerdes, R.: Landfast ice affects the stability of the A rctic halocline: Evidence from a numerical model, Journal of Geophysical Research: Oceans, 120, 2622–2635, 2015.

Jensen, D., Mahoney, A., and Resler, L.: The annual cycle of landfast ice in the eastern Bering Sea, Cold Regions Science and Technology, 174, 103 059, 2020.

Jones, J., Eicken, H., Mahoney, A., Rohith, M., Kambhamettu, C., Fukamachi, Y., Ohshima, K. I., and George, J. C.: Landfast sea ice breakouts: Stabilizing ice features, oceanic and atmospheric forcing at Barrow, Alaska, Continental Shelf Research, 126, 50–63, 2016.

Kaleschke, L., Tian-Kunze, X., Maaß, N., Mäkynen, M., and Drusch, M.: Sea ice thickness retrieval from SMOS brightness temperatures during the Arctic freeze-up period, Geophysical Research Letters, 39, 2012.

Kasper, J. L. and Weingartner, T. J.: The spreading of a buoyant plume beneath a landfast ice cover, Journal of Physical Oceanography, 45, 478–494, 2015.

Khalilian, V.: A fog and low visibility climatology for selected stations in the Western Canadian Arctic, Ph.D. thesis, 2016.

Kwok, R., Cunningham, G. F., Wensnahan, M., Rigor, I., Zwally, H. J., and Yi, D.: Thinning and volume loss of the Arctic Ocean sea ice cover: 2003–2008, Journal of Geophysical Research: Oceans, 114, https://doi.org/10.1029/2009JC005312, 2009.

Kwok, R., Markus, T., Kurtz, N., Petty, A., Neumann, T., Farrell, S., Cunningham, G., Hancock, D., Ivanoff, A., and Wimert, J.: Surface height and sea ice freeboard of the Arctic Ocean from ICESat-2: Characteristics and early results, Journal of Geophysical Research: Oceans, 124, 6942–6959, 2019.

Laidler, G. J., Ford, J. D., Gough, W. A., Ikummaq, T., Gagnon, A. S., Kowal, S., Qrunnut, K., and Irngaut, C.: Travelling and hunting in a changing Arctic: Assessing Inuit vulnerability to sea ice change in Igloolik, Nunavut, Climatic change, 94, 363–397, 2009.

Laidre, K. L., Stirling, I., Lowry, L. F., Wiig, Ø., Heide-Jørgensen, M. P., and Ferguson, S. H.: Quantifying the sensitivity of Arctic marine mammals to climate-induced habitat change, Ecological applications, 18, S97–S125, 2008.

Lantuit, H. and Pollard, W.: Fifty years of coastal erosion and retrogressive thaw slump activity on Herschel Island, southern Beaufort Sea, Yukon Territory, Canada, Geomorphology, 95, 84–102, 2008.

Laxon, S. W., Giles, K. A., Ridout, A. L., Wingham, D. J., Willatt, R., Cullen, R., Kwok, R., Schweiger, A., Zhang, J., Haas, C., et al.: CryoSat-2 estimates of Arctic sea ice thickness and volume, Geophysical Research Letters, 40, 732–737, 2013.

Lemieux, J.-F., Tremblay, L. B., Dupont, F., Plante, M., Smith, G. C., and Dumont, D.: A basal stress parameterization for modeling landfast ice, Journal of Geophysical Research: Oceans, 120, 3157–3173, 2015.

Lovvorn, J. R., Rocha, A. R., Mahoney, A. H., and Jewett, S. C.: Sustaining ecological and subsistence functions in conservation areas: eider habitat and access by Native hunters along landfast ice, Environmental Conservation, 45, 361–369, 2018.

Magruder, L. A., Reese, A. R., Gibbons, A., Dietrich, J. T., and Neumann, T. A.: ICESat-2 Onboard Flight Receiver Algorithms: On-orbit Parameter Updates the Impact on Science Driven Observations, 2024.

https://doi.org/10.5194/egusphere-2024-1885
Preprint. Discussion started: 1 July 2024

Mahoney, A., Eicken, H., Gaylord, A. G., and Shapiro, L.: Alaska landfast sea ice: Links with bathymetry and atmospheric circulation, Journal of Geophysical Research: Oceans, 112, 2007a.

Mahoney, A., Eicken, H., and Shapiro, L.: How fast is landfast sea ice? A study of the attachment and detachment of nearshore ice at Barrow, Alaska, Cold Regions Science and Technology, 47, 233–255, 2007b.

Mahoney, A., Gearheard, S., Oshima, T., and Qillaq, T.: Sea ice thickness measurements from a community-based observing network, Bulletin of the American Meteorological Society, 90, 370–378, 2009.

Mahoney, A. R.: Alaska landfast sea ice dynamics, University of Alaska Fairbanks, 2006.

Mahoney, A. R., Eicken, H., Gaylord, A. G., and Gens, R.: Landfast sea ice extent in the Chukchi and Beaufort Seas: The annual cycle and decadal variability, Cold Regions Science and Technology, 103, 41–56, 2014.

Markus, T., Neumann, T., Martino, A., Abdalati, W., Brunt, K., Csatho, B., Farrell, S., Fricker, H., Gardner, A., Harding, D., et al.: The Ice, Cloud, and land Elevation Satellite-2 (ICESat-2): science requirements, concept, and implementation, Remote sensing of environment, 190, 260–273, 2017.

Masterson, D.: State of the art of ice bearing capacity and ice construction, Cold Regions Science and Technology, 58, 99–112, 2009.

Maykut, G. and Untersteiner, N.: The geophysics of sea ice, New York, Plenium, 1986.

McGonigal, D. and Barrette, P. D.: A field study of grounded ice features and associated seabed gouging in the Canadian Beaufort Sea, Cold Regions Science and Technology, 146, 142–154, 2018.

Meier, W. N., Stroeve, J., and Gearheard, S.: Bridging perspectives from remote Sensing and Inuit communities on changing Sea-ice cover in the Baffin Bay region, Annals of Glaciology, 44, 433–438, https://doi.org/10.3189/172756406781811790, 2006.

Meyer, F. J., Mahoney, A. R., Eicken, H., Denny, C. L., Druckenmiller, H. C., and Hendricks, S.: Mapping arctic landfast ice extent using L-band synthetic aperture radar interferometry, Remote Sensing of Environment, 115, 3029–3043, 2011.

NOAA: Tides and Currents: Barrow Offshore, AK - Station ID: 9494935, https://tidesandcurrents.noaa.gov/noaatidepredictions.html?id=9494935&legacy=1, 2010.

NOAA: Global Historical Climatology Network-hourly (GHCNh), Version 1: Subset 69 to 72N, 163 to 143 W, https://www.ncei.noaa.gov/access/search/data-search/global-historical-climatology-network-hourly?dataTypes=temperature&pageNum=1&startDate=2021-10-01T00:00:00&endDate=2022-05-31T23:59:59&bbox=72.000,-163.000,69.000,-143.000, 2024.

Overeem, I., Anderson, R. S., Wobus, C. W., Clow, G. D., Urban, F. E., and Matell, N.: Sea ice loss enhances wave action at the Arctic coast, Geophysical Research Letters, 38, 2011.

Overland, J. E., Wang, M., Walsh, J. E., and Stroeve, J. C.: Future Arctic Climate Changes: Adaptation anfd Mitigation Time Scales, Earth's Future, 2, 68–74, 2014.

Petrich, C., Eicken, H., Zhang, J., Krieger, J., Fukamachi, Y., and Ohshima, K. I.: Coastal landfast sea ice decay and breakup in northern Alaska: Key processes and seasonal prediction, Journal of Geophysical Research: Oceans, 117, 2012.

Potter, R., Walden, J., and Haspel, R.: Design and construction of sea ice roads in the Alaskan Beaufort Sea, in: Offshore Technology Conference, pp. OTC–4080, OTC, 1981.

Reimnitz, E., Toimil, L., and Barnes, P.: Arctic continental shelf morphology related to sea-ice zonation, Beaufort Sea, Alaska, Marine Geology, 28, 179–210, 1978.

Ricker, R., Fons, S., Jutila, A., Hutter, N., Duncan, K., Farrell, S. L., Kurtz, N. T., and Fredensborg Hansen, R. M.: Linking scales of sea ice surface topography: evaluation of ICESat-2 measurements with coincident helicopter laser scanning during MOSAiC, The Cryosphere, 17, 1411–1429, 2023.

https://doi.org/10.5194/egusphere-2024-1885
Preprint. Discussion started: 1 July 2024

Rothrock, D. A., Yu, Y., and Maykut, G. A.: Thinning of the Arctic sea-ice cover, Geophysical Research Letters, 26, 3469–3472, 1999.

Selyuzhenok, V., Krumpen, T., Mahoney, A., Janout, M., and Gerdes, R.: Seasonal and interannual variability of fast ice extent in the southeastern L aptev S ea between 1999 and 2013, Journal of Geophysical Research: Oceans, 120, 7791–7806, 2015.

Selyuzhenok, V., Mahoney, A., Krumpen, T., Castellani, G., and Gerdes, R.: Mechanisms of fast-ice development in the south-eastern Laptev Sea: a case study for winter of 2007/08 and 2009/10, Polar Research, 36, 1411 140, 2017.

Stammerjohn, S., Massom, R., Rind, D., and Martinson, D.: Regions of rapid sea ice change: An inter-hemispheric seasonal comparison, Geophysical Research Letters, 39, 2012.

Strub-Klein, L. and Sudom, D.: A comprehensive analysis of the morphology of first-year sea ice ridges, Cold Regions Science and Technology, 82, 94–109, 2012.

UAF: University of Alaska Fairbanks. Barrow Sea Ice Radar, https://seaice.alaska.edu/gi/observatories/barrow_radar/, accessed: 2024, 2022.

Yu, Y., Stern, H., Fowler, C., Fetterer, F., and Maslanik, J.: Interannual variability of Arctic landfast ice between 1976 and 2007, Journal of Climate, 27, 227–243, 2014.

Zhang, X., Walsh, J. E., Zhang, J., Bhatt, U. S., and Ikeda, M.: Climatology and interannual variability of Arctic cyclone activity: 1948–2002, Journal of climate, 17, 2300–2317, 2004.

Zhao, Y. and Liu, A. K.: Arctic sea-ice motion and its relation to pressure field, Journal of oceanography, 63, 505–515, 2007.